Self-Assembly of Recombinant Amphiphilic Oligopeptides into Vesicles

Albert J. van Hell,[†] Cristina I. C. A. Costa,[†] Frits M. Flesch,[†] Marc Sutter,[‡] Wim Jiskoot,[‡] Daan J. A. Crommelin,[†] Wim E. Hennink,[†] and Enrico Mastrobattista*,[†]

Department of Pharmaceutics, Utrecht Institute for Pharmaceutical Sciences, Utrecht University, P.O. Box 80082, 3508 TB Utrecht, The Netherlands, and Division of Drug Delivery Technology, Leiden/Amsterdam Center for Drug Research, Leiden University, P.O. Box 9502, 2300 RA Leiden, The Netherlands

Received April 19, 2007; Revised Manuscript Received June 14, 2007

The aim of the present study was to design amphiphilic oligopeptides that can self-assemble into vesicular structures. The ratio of hydrophilic to hydrophobic block length was varied, and peptides were designed to have a hydrophobic tail in which the bulkiness of the amino acid side groups increases toward the hydrophilic domain (Ac-Ala−Ala-Val-Val-Leu-Leu-Leu-Trp-$Glu_{2/7}$-COOH). These peptides were recombinantly produced in bacteria as an alternative to solid-phase synthesis. We demonstrate with different complementary techniques (dynamic and static light scattering, tryptophan fluorescence anisotropy, and electron microscopy) that these amphiphilic peptides spontaneously form vesicles with a radius of approximately 60 nm and a low polydispersity when dispersed in aqueous solution at neutral pH. Morphology and size of the vesicles were relatively insensitive to the variations in hydrophilic block length. Exposure to acidic pH resulted in formation of visible aggregates, which could be fully reversed to vesicles upon pH neutralization. In addition, it was demonstrated that water-soluble molecules can be entrapped inside these peptide vesicles. Such peptide vesicles may find applications as biodegradable drug delivery systems with a pH-dependent release profile.

Introduction

The self-assembly of biomolecules has gained increasing attention as a means to design novel biomaterials from biomolecular building blocks (e.g., DNA, proteins, and peptides).[1,2] A variety of supramolecular structures have been formed with self-assembling peptides, such as macroscopic hydrogels,[3−5] fibers,[6] β-sheet tapes,[7] polypeptide vesicles,[8,9] and nanotubes.[10,11] The biocompatability of peptide assemblies is underscored by their successful utilization in various biological and medical applications, such as stem cell differentiation, tissue engineering, in vivo nerve regeneration, and scaffolds to deposit hydroxyapatite minerals as a mimic for extracellular bone matrix.[12−16]

Zhang et al. showed that small amphiphilic oligopeptides self-assembled into nanotubes.[10,11,17,18] They proposed a model of assembly in which the peptides stick together tail-to-tail, forming a bilayer similar to lipids in an aqueous environment.[10,18] These peptides were found to predominantly assemble into open-ended tubes. A vesicular architecture, however, might be useful in a variety of applications, for example, to encapsulate and deliver pharmaceutically active compounds, such as low-molecular-weight drugs as well as biotherapeutics (protein, siRNA, and pDNA).[19,20]

Extensive research about the self-assembling behavior of amphiphiles has provided valuable information about critical parameters determining the final assembled architecture. The surface area occupied by a monomer, relative to the length of the hydrophobic block, determines the packaging shape of a monomer within a supramolecular assembly.[21] A slightly increased surface area is favorable for the formation of vesicles, when compared to the formation of planar bilayers.[22,23] Besides the size and charge of the hydrophilic residues, such a surface area is influenced by the length of the hydrophilic block; an extension of the hydrophilic block favors an increase of occupied surface area per monomer.[24,25] Therefore, the ratio of hydrophobic to hydrophilic block length can be varied to obtain a vesicular architecture.[26]

The aim of the current study was to develop amphiphilic oligopeptides that self-assemble into vesicles in an aqueous environment. Two peptides were designed to be amphipatic and negatively charged at a neutral pH and to occupy a relatively large interfacial surface area. These self-assembling (SA) peptides were recombinantly produced in bacteria as an alternative to solid-phase synthesis, a production route that might be advantageous, for example, for large scale production.[27] After purification and N-terminal acetylation, these peptides were characterized for their self-assembling behavior by fluorescence spectroscopy, electron microscopy, and dynamic and static light scattering.

Experimental Section

DNA Design and Construction. Oligo DNA 5′-GCGGCGGTG-GTGCTGCTGCTGTGGGAAGAA(G/T)AA(G/T)AA(G/T)AA TGAT-AGACTCGGATCC-3′ and 5′-GCGGCGGTGGTGCTGCTGCTGTGG-GAAGAAGAAGAA(G/T)AA(G/T)AA(G/T)AATGATAGACTCG-GATCC-3′ were made double-stranded by annealing 5′-TTCGGA-TCCGAGTCTA-3′ oligo DNA and strand extension by incubation at 65 °C with Taq polymerase (Fermentas, Burlington, Canada), generating adenine overhangs. The double-stranded DNA was directly ligated in pET SUMO plasmid (Invitrogen, Carlsbad, CA) by TA cloning, and the constructs were transformed into *Escherichia coli* strain

* Author to whom correspondence should be addressed. Phone: +31-30-2539392. Fax: +31-30-2517839. E-mail: E.Mastrobattista@uu.nl.
[†] Utrecht University.
[‡] Leiden University.

10.1021/bm0704267 CCC: $37.00
Published on Web 08/14/2007

Mach1 T1 competent cells (Invitrogen, Carlsbad, CA) for colony screening. Correct insertion of oligo DNA was confirmed by DNA sequencing.

Protein and Peptide Biosynthesis and Purification. The *E. coli* strain BL21(DE3) (Invitrogen Carlsbad, CA) was transformed with the constructed DNA plasmids to express the SUMO−SA fusion proteins. Five liters of Luria−Bertani (LB) medium, supplemented with 10 μg/mL kanamycin and trace metal solution,[28] was inoculated with a 100 mL overnight shaking-flask bacterial culture in LB medium. Bacteria were grown in a Labfors 3 fermentor (Infors HT, Bottmingen, Switzerland) with air flow, pH (7.0), and temperature (37 °C) control and growth-dependent glucose supply. Protein expression was induced by addition of isopropyl-β-D-thiogalactopyranoside (IPTG) (Fisher Emergo, Landsmeer, The Netherlands) to a final concentration of 1 mM. Three hours after induction, cells were harvested by centrifugation. Bacterial pellets were resuspended in lysis buffer (150 mM NaCl, 20 mM NaH_2PO_4, 10 mM imidazole, pH 8.0). Lysis was performed by a single cycle of freezing and thawing of the bacteria, 30 min of incubation with lysozyme (1 mg/mL) at ambient temperature, and subsequent sonication on ice, using a Braun Labsonic tip-sonicator (Braun Biotech, Melsungen, Germany). Bacterial lysates were centrifuged (30 min, 70 000*g*, 5 °C), the and supernatant was filtered through a 0.45 μm syringe filter. SUMO−SA fusion proteins were captured from the cleared lysate using an Akta Purifier equipped with 5 mL His-Trap HP columns (GE Healthcare, Uppsala, Sweden). After capture, the columns were washed extensively (25 column volumes of 1.1 M NaCl and 25 column volumes of 50 mM imidazole), and His-tagged protein was eluted at 400 mM imidazole (150 mM NaCl, 20 mM NaH_2PO_4, 400 mM imidazole, pH 8.0). The elution buffer was exchanged to SUMO protease cleavage buffer (20 mM HEPES, 150 mM NaCl, 1 mM dithiothreitol (DTT), pH 8.0) using a HiPrep 26/10 desalting column (GE Healthcare, Uppsala, Sweden). To release the peptides 1 unit of SUMO protease (Invitrogen, Carlsbad, CA) per milliliter of protein solution was added and incubated at ambient temperature for 6 h. Cleavage was confirmed by size exclusion chromatography on a Superdex Peptide 10/300 GL column (GE Healthcare, Uppsala, Sweden) at a flow rate of 0.5 mL/min with phosphate-buffered saline (pH 7.4) as a mobile phase. Column performance was determined with a Gel Filtration LMW Calibration kit (GE Healthcare, Uppsala, Sweden). A second immobilized metal affinity chromatography (IMAC) purification was performed with 5 mL nickel−nitrilotriacetic acid (Ni−NTA) Superflow (Qiagen, Hilden, Germany) to remove both the His-tagged SUMO protease and protein.

Gel Electrophoresis. For sodium dodecyl sulfate polyacrylamide gel electrophoresis (SDS-PAGE), samples were boiled in Laemmli sample buffer (Bio-Rad Laboratories, Hercules, CA) for 5 min and loaded to a 15% acrylamide gel. Electrophoresis was performed at room temperature, applying 10 mA per gel until the running front reached the end. The gel was fixed in 50% methanol and 12% acetic acid, and the bands were visualized by silver staining. Mark 12 protein standard (Invitrogen, Carlsbad, CA) was used as a reference.

Peptide Acetylation and Self-Assembly. The N-termini of the peptides were acetylated by incubating the purified peptide in 25% acetic anhydride, 50% methanol, and 25% water (volume) for 1 h at ambient temperature.[29] The extent of acetylation was determined with a 2,4,6-trinitrobenzene sulfonic acid assay (Pierce, Rockford, IL), measuring UV absorbance at 335 nm, according to the manufacturer's protocol. Solvents were removed by reduced pressure evaporation, and the remaining peptides were washed once in H_2O as follows: Peptides were rehydrated and subsequently precipitated by acidification. The precipitated peptides were harvested by centrifugation (30 min at 17 000*g*). Self-assembly of the peptides was performed by dispersing the precipitated peptide in 1 mM NaOH in H_2O while gently shaking (pH > 7). Peptide dispersions were centrifuged for 5 min at 13 000*g* to sediment any dust particles present. The peptide concentration was determined by UV measurements at 280 nm based on the molar extinction coefficient of the tryptophan residue (5690 M^{-1} cm^{-1}).

High-Performance Liquid Chromatography (HPLC) Analysis and Mass Spectrometry. Acetylated peptide was injected onto a Sunfire C18 column (Waters Corporation, Milford, MA). A gradient was run at flow rate of 1 mL/min from 5% acetonitrile, 0.1% trifluoroacetic acid, and 95% water in 30 min to 95% acetonitrile, 0.1% trifluoroacetic acid, and 5% water and ran an additional 10 min as such. UV absorbance was monitored at $\lambda = 280$ nm. Online electron spray ionization mass spectrometry (ESI-MS) in positive ion mode was performed on a Finnigan LCQ Deca MAX (Thermo Electron Corporation, Waltham, MA).

Fluorescence Anisotropy. To determine the critical aggregate concentration (CAC) of the peptides, dilution series of the peptide (1000−0.1 μg/mL) were prepared in 10 mM phosphate buffer (pH 8.0). Tryptophan steady-state fluorescence anisotropy was measured with a Horiba Fluorolog fluorometer (Horiba Jobin Yvon, Longjumeau Cedex, France) using quartz cuvettes (Hellma, Müllheim, Germany). Experiments were performed at 22 °C. Samples were excited at 290 nm, and emission was recorded at 360 nm. An integration time of 10 s was used, and the excitation and emission band slits were set at 7 and 10 nm, respectively. The fluorescence intensities I_{VV} and I_{VH} were measured with the polarizers of the instrument in vertical−vertical (VV) and vertical−horizontal (VH) positions, respectively. The anisotropy (r) was calculated from the measured intensities I_{VV} and I_{VH} using

$$r = (I_{VV} - GI_{VH})/(I_{VV} + 2GI_{VH}) \quad (1)$$

The factor G corrects for differences in the sensitivity of the detection system of vertically and horizontally polarized light and was determined with peptide samples at concentrations below the CAC by using

$$G = I_{HV}/I_{HH} \quad (2)$$

where I_{HV} and I_{HH} are the fluorescence intensities with the polarizers in horizontal−vertical (HV) and horizontal−horizontal (HH) positions, respectively. For each peptide anisotropy was plotted against the peptide concentration.

Cryogenic Transmission Electron Microscopy. Cryogenic transmission electron microscopy (TEM) analysis was performed on 1 and 3 mg/mL peptide dispersions. Quick freezing of the samples was performed using a Vitrobot (FEI Company, Eindhoven, The Netherlands). Samples were applied on glow-discharged 200 mesh grids, covered with Quantifoil holey carbon foil (Micro Tools GmbH, Jena, Germany), and blotted for 0.5 s at 100% relative humidity. Immediately the samples were vitrified by plunging the grid into liquid ethane and subsequently placed in dry liquid nitrogen. Grids were introduced into a Tecnai12 transmission electron microscope (Philips, Eindhoven, The Netherlands) using a GATAN 626 cryoholder (Gatan GmbH, München, Germany). Samples were observed at 120 kV with low-dose imaging conditions to avoid melting of the vitrified film. Images were recorded on a TemCam-0124 camera (TVIPS GmBH, Gauting, Germany) and processed with AnalySIS software.

Zeta Potential and Light Scattering Techniques. Buffers used to dilute the peptide dispersions were filtered through 0.02 μm filters (Whatman, Kent, U. K.). Static light scattering (SLS) and dynamic light scattering (DLS) measurements were performed in a Malvern ALV CGS-3 goniometer (Malvern Instruments, Malvern, U. K.) containing a He−Ne laser source ($\lambda = 632.8$ nm, 22 mW output power). The DLS time correlation was analyzed by ALV Correlator 3.0 software (ALV, Langen, Germany). For pH-dependent DLS measurements 10 mM citrate buffer was used. pH values were adjusted with 1.0 M HCl or 1.0 M NaOH. SLS was performed at angles between 150° and 30° for four different peptide concentrations (40, 50, 60, and 80 μg/mL). A Guinier plot was constructed using ALVStat 4.31 software (ALV, Langen, Germany), and the molecular weight of the vesicles was obtained,using the dn/dc of peptides in HEPES buffer (0.185 mL/g).[30] The dn/dc of the vesicle interior was assumed to be similar to the buffer. The particle aggregation number was calculated by dividing the particle molecular weight by the molecular weight of the peptide monomer.

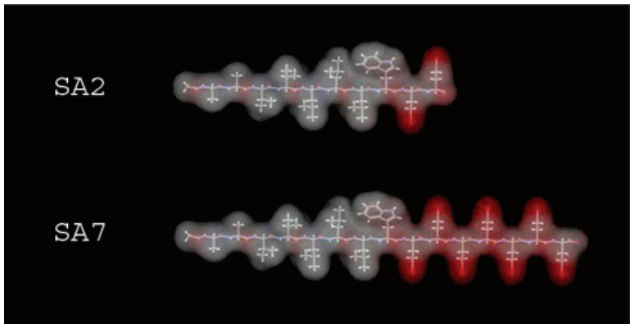

Figure 1. Space-filling molecular models of stretched SA peptides, exhibiting a conically shaped hydrophobic domain (amino acid sequence, Ac-Ala-Ala-Val-Val-Leu-Leu-Leu-Trp-Glu_{2-7}-COOH). Apolar regions are depicted in gray; charged species are depicted in red.

Zeta potential measurements were performed in 5 mM HEPES (pH 8.0) in a dip-in cell on a Zetasizer 2000 (Malvern Instruments, Malvern, U. K.).

Calcein Encapsulation Assay. Spin columns containing 250 mg of Sephadex G50 (medium bead size; Amersham Bioscience, Uppsala, Sweden) were prepared according to Fry et al.[31] SA2 peptides precipitated by acidification were dispersed in the absence or presence of a 4 mM calcein solution in HEPES buffer (5 mM HEPES, pH 8.0). Fifty microliters of the peptide dispersion (0.2 mg/mL) were then applied to the spin column and subsequently spun for 3 min at 350*g* in a swing-out rotor, and the eluent was collected. Consecutive elution steps (applying 50 μL of hepes buffer followed by centrifugation at 350*g* for 3 min) were performed, and the eluted fractions were collected and analyzed for calcein fluorescence using a Fluorostar Optima microplate reader (BMG Labtech GmbH, Offenburg, Germany) set at 488 nm excitation and 514 nm emission wavelengths. As a reference, egg phosphatidylglycerol (EPG) liposomes were prepared in HEPES buffer containing 4 mM calcein by lipid-film hydration and extrusion as described by Olson et al.[32] After extrusion the average size of the EPG liposomes was 45 nm in radius with a polydispersity index (PDI) of 0.17. The liposome sample was adjusted to give a similar light scattering intensity as the peptide dispersion prior to loading 50 μL onto the spin column.

Results

Peptide Design. SA2 and SA7 peptides were designed to be amphipathic, containing glutamic acid residues as the hydrophilic domain (Figure 1) that, due to their side chain size and electrostatic repulsion, will occupy a relatively large interfacial area. A relative increase in hydrophilic block length also may enlarge the surface area.[24] Therefore, the mass fraction of the hydrophilic block was varied from 25% (SA2) to 50% (SA7) of total peptide mass, while keeping the length of hydrophobic domain unchanged. In the hydrophobic domain of the SA peptides a conical shape was introduced by using hydrophobic amino acids with decreasing bulkiness of the side chains toward the N-terminus (Figure 1). Tryptophans are well-suited to a polar−apolar interphase, due to the polarity of the amide group present in the further hydrophobic indole side chain.[33] The N-terminus of the peptide was acetylated to prevent undesired charge interactions with the negatively charged glutamic acid residues and to increase hydrophobicity.[34]

Recombinant Production and Purification of Amphiphilic Peptides. The amphiphilic oligopeptides SA2 and SA7 were recombinantly produced as a cost-effective alternative to solid-phase synthesis. To prevent degradation or toxicity of the unfolded, amphiphilic peptides in bacteria, SUMO protein was used as a fusion protein that has been reported to increase the solubility and yield of recombinant proteins.[35−37] DNA constructs, encoding the different SA peptides (Figure 1), were cloned into the pET-SUMO vector in frame with and downstream of the SUMO gene. The resulting gene constructs were expressed in *E. coli* strain BL21(DE3). The SUMO fusion protein contained an N-terminal hexahistidine tag that allowed purification by IMAC. The SA peptide was cleaved from the C-terminus of the SUMO protein by SUMO protease, which cleaves by recognizing the three-dimensional structure of the SUMO protein rather than a specific amino acid (sequence), yielding SA peptides without any undesired amino acids on their N-termini.[37]

A typical example of SA peptide production in *E. coli* is shown in Figure 2. Total protein content of the BL21(DE3) bacteria expressing SUMO−SA2 fusion proteins was analyzed on a SDS-PAGE gel, before and after induction of recombinant protein expression with IPTG (Figure 2A). In the IPTG-treated sample, a protein band with an apparent molecular weight of ca. 17 kDa appeared, which is close to the theoretical mass of the fusion protein (13 kDa). After 3 h of induction by IPTG, ~40% of the soluble fraction of the bacterial proteins consisted of the SUMO−peptide (SUMO−SA2) fusion protein (Figure 2A, third lane). One-step IMAC was performed to purify the fusion protein from the soluble fraction of the bacterial lysate (Figure 2A, fourth lane). From the purified fusion protein the imidazole was removed by a desalting step, and the protein was incubated with SUMO protease to release the SA peptide. Cleavage is clearly visualized by monitoring the release of protein (UV absorbance at 280 nm) from a Superdex peptide column (Figure 2B) (void volume peak no. 1, optimal separation range 1−15 kDa) before (line A) and after cleavage by SUMO protease (line B). After cleavage a low-molecular-weight peak appeared (peak 3) that corresponded to the SA2 peptide as was revealed by MS analysis. The cleavage efficiency depended on incubation time and temperature. After 6 h of incubation at ambient temperature, cleavage was complete. In the void volume of the column (peak 1) some copurified bacterial proteins and aggregated fusion proteins came off. However, by application of the mixture of cleaved SA peptide on a Ni−NTA column, the copurified proteins, the His-tagged SUMO protease, and the SUMO fusion protein were removed and yielded the SA peptides (line C, Figure 2B). The purified SA peptide was acetylated on its N-terminus and analyzed by reverse-phase chromatography (Figure 2C) and subsequently with ESI-MS (Figure 2D). The observed mass of *N*-acetyl-SA2 was 1184.58 Da, which is in good agreement with the expected mass of 1183.65 Da (Figure 2D). Non-acetylated peptide was neither detected by ESI-MS nor by the free-amine-sensitive 2,4,6-trinitrobenzene sulfonic acid assay. SA7 peptide was produced in the same way. Typically, from a 5 L fermentation (25 g of bacteria, dry cell weight), 300 mg of purified fusion protein was obtained, which yielded 30 mg of acetylated SA peptide.

CAC Determination. After purification and subsequent acetylation of their N-termini, the SA peptides were studied for their self-assembling behavior in aqueous solution. To investigate the CAC of the peptide assemblies, tryptophan fluorescence anisotropy was used. Steady-state anisotropy is a measure of the rotational motion of fluorophores.[38] At the CAC, the average rotational rate of the peptide molecules and of their intrinsic tryptophan residues will decrease abruptly, because of formation of peptide assemblies. This will manifest itself as a sudden increase of intrinsic tryptophan anisotropy.[39]

As can be seen in Figures 3 A and 3B, both peptide dispersions displayed a sharp rise of anisotropy with increasing peptide concentrations. This allowed determination of the CAC,

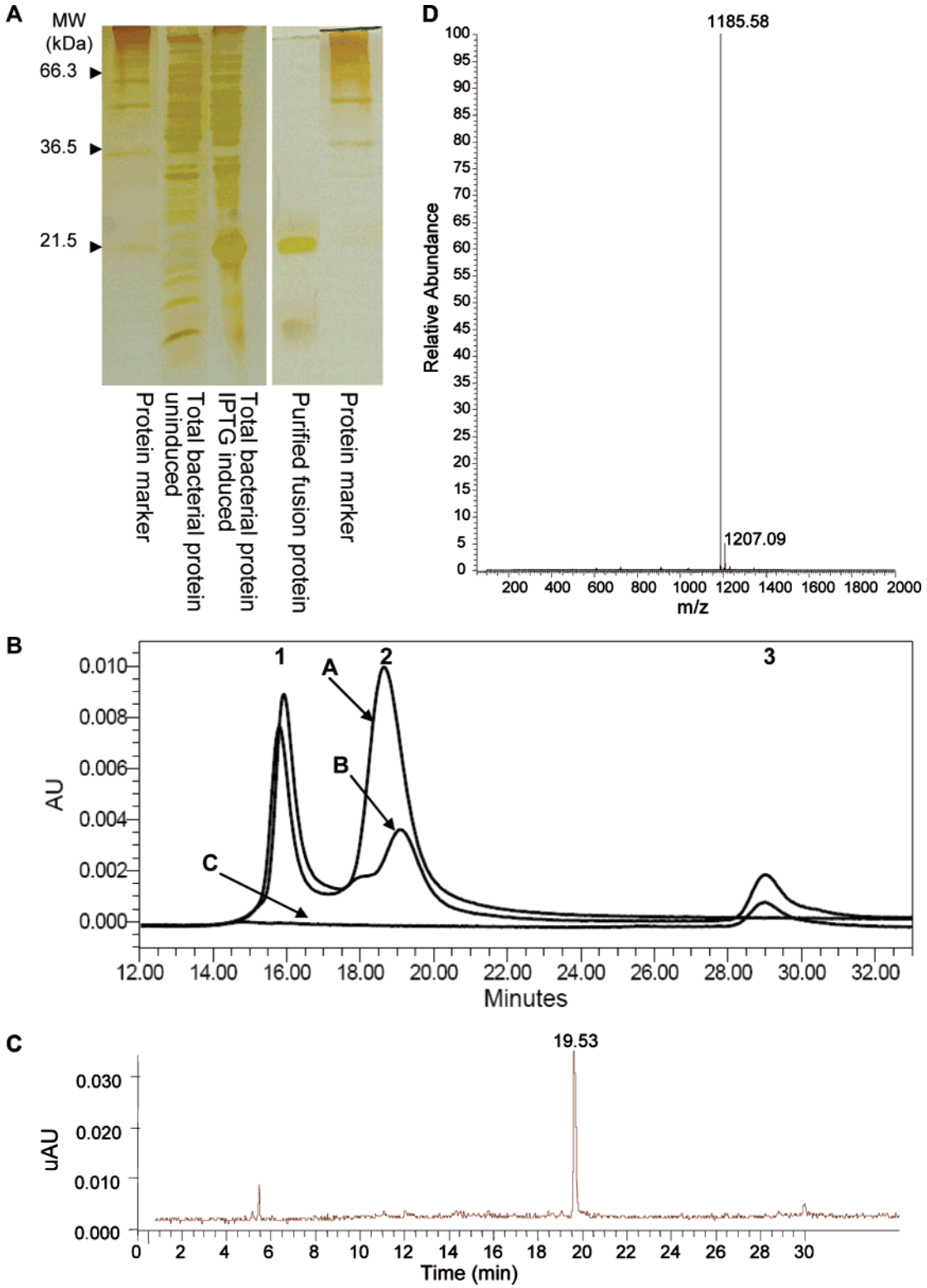

Figure 2. Recombinant production of SA2 oligopeptide in *E. coli* BL21(DE3). (A) Expression and subsequent purification of the SUMO−SA2 peptide fusion protein, analyzed on a 15% SDS-PAGE and visualized by silver staining. Lanes 1 and 5: Mark 12 protein standard (Invitrogen). Lane 2: Total bacterial protein, uninduced. Lane 3: Total bacterial protein, IPTG-induced protein expression. Lane 4: IMAC-purified SUMO−SA2 fusion protein. (B) Enzymatic release of the SA2 peptide from the SUMO fusion protein using SUMO protease, analyzed by size exclusion chromatography (Superdex Peptide 10/300 GL column with UV absorbance monitored at 280 nm). SUMO fusion protein (peak 2) before (line A) and after (line B) incubation with SUMO protease. The cleaved peptide (peak 3) was purified by removing copurified proteins (peak 1), the SUMO fusion protein, and the SUMO protease, both bearing hexahistidine tags, with IMAC (line C). (C) HPLC analysis on the purified and acetylated SA peptide, UV absorbance monitored at 280 nm. (D) ESI mass spectrum of the 19.53 min peak in part C (19.47−19.84 min, expected mass 1183.65 Da).

which is defined at the intersection of a linear fit through the points at low anisotropy values and a linear fit through the points describing a steep anisotropy increase. The CAC determined in this way was found to be 4.9×10^{-7} M for SA2, whereas the CAC of SA7 was 1.6×10^{-5} M. Measurements with a SA5 peptide, containing an identical hydrophobic block as SA2 and

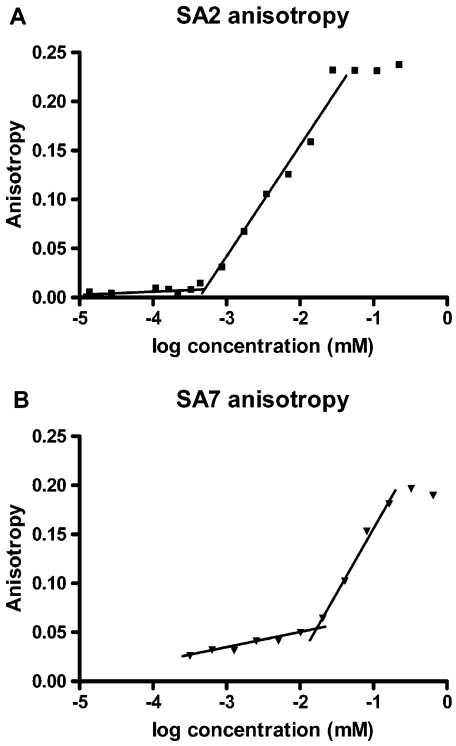

Figure 3. Tryptophan steady-state anisotropy as a function of (A) SA2 and (B) SA7 peptide concentration. The CAC was determined at the intersection of the two linear fits in parts A (SA2; 4.9×10^{-7} M) and B (SA7; 1.6×10^{-5} M).

SA7 and five glutamic acid residues, gave a CAC of 1.3×10^{-6} M (data not shown). This confirms that there is a trend for increasing CAC with increasing length of the hydrophilic block of the peptide. In the case of minimal rotational movement of tryptophans, the maximal anisotropy value in isotropic solution is near 0.3.[38] The SA2 peptide assemblies, however, display a plateau value of around 0.23, and for SA7 assemblies the maximal anisotropy value seems even somewhat lower. These maximal values indicate that some local rotational motion of the tryptophan residues is allowed within the assemblies.

Morphology of the Peptide Self-Assemblies. Transmission electron microscopy was used to elucidate the morphology of the SA2 and SA7 peptide assemblies (Figure 4). The use of the quick-freeze technique with subsequent TEM provides an impression of the particles in solution and avoids potential artifacts induced by staining of the sample. As can be seen in Figure 4, the assemblies were situated apart, while others were attached or overlapping (SA5; Figure 4D). All assemblies appeared as spherical particles, and neither tubes nor fibrils were observed. As can be seen at a higher magnification a rim of extra contrast clearly encircles the spheres (Figure 4D). These observations are not due to the instrument being out-of-focus, since that would result in a vague, bright rim, instead of the dark, thin line that is present around the spheres. The morphology of the particles was insensitive to increased hydrophilic block length, since for SA2 (Figures 4A and 4C) and SA7 (Figure 4B) only spherical particles of comparable sizes were observed. Peptide particles were also visualized with atomic force microscopy (AFM) by immobilization of the particles on an ornithine-modified silica matrix (Figure S1 of the Supporting Information), showing similar morphologies and size distributions as seen with TEM. The spherically assembled peptide structures exhibit a relatively soft nature, since minor forces were needed to destroy the peptide assemblies by the AFM cantilever.

Dynamic and Static Light Scattering and Zeta Potential Measurements. The SA2 and SA7 assemblies were analyzed by DLS to obtain the hydrodynamic radius (R_h) of the assemblies

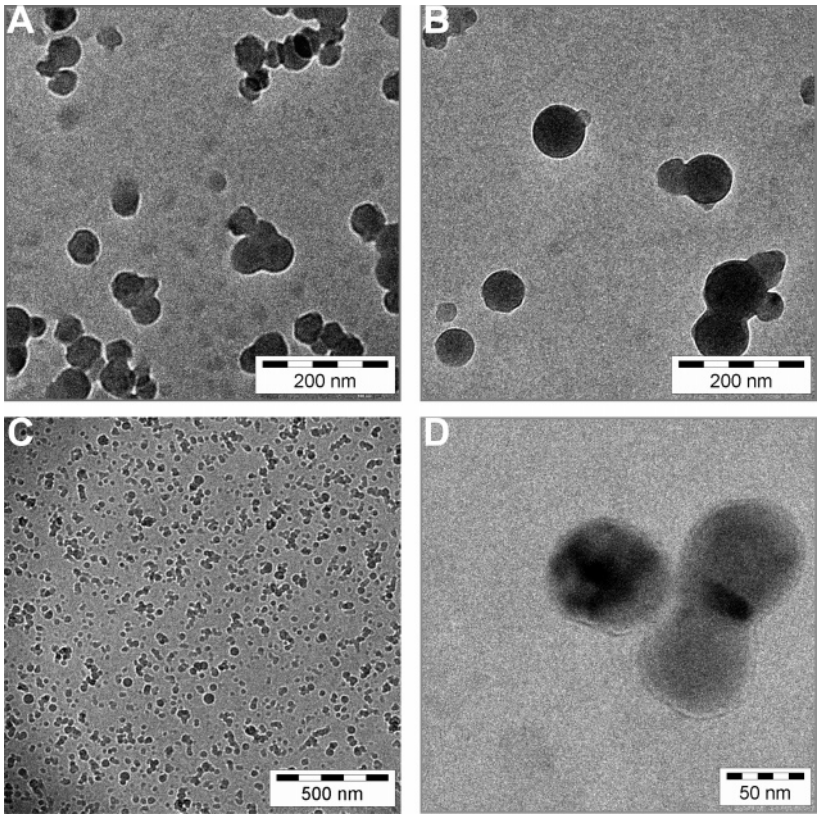

Figure 4. Transmission electron microscopy of peptide self-assemblies. (A) SA2, (B) SA7, and (D) SA5 peptides yielded spherical assemblies only. The spheres are abundantly present in solution (C; overview of SA2 assemblies).

Table 1. Macromolecular Properties of the Peptide Assemblies

	zeta potential (mV)	R_h[a] (nm)	polydispersity index	R_g[b] (nm)	ρ parameter	particle molecular weight	aggregation number	surface area per monomer (nm^2)
SA2	−48 (±1)	63 (±1)	0.21	66 (±2)	1.04 (±0.03)	$3.0\ (\pm0.1) \times 10^7$	$2.5\ (\pm0.1) \times 10^4$	4.0 (±0.2)
SA7	−26 (±1)	59 (±3)	0.24	54 (±1)	0.92 (±0.06)	$1.8\ (\pm0.1) \times 10^7$	$9.8\ (\pm0.2) \times 10^3$	8.9 (±0.6)

[a] Hydrodynamic radius. [b] Radius of gyration.

(Table 1). The radii found (63 nm for SA2 and 59 nm for SA7) correspond to the largest particles observed in EM micrographs (Figure 4). The particle sizes were stable over time (>3 months, 4 °C) and at physiological conditions (150 mM sodium chloride, 10 mM sodium phosphate, pH 7.4). The PDIs of the self-assemblies were between 0.21 and 0.24, which indicate little heterogeneity of particle size, as was also observed by TEM.

Static light scattering provides information about the radius of gyration (R_g) and the molecular weight of the particles. Results of SLS data analysis are shown in Table 1. The ρ-parameter (R_g/R_h) sheds light onto the density distribution of the particles and thereby on particle morphology.[40] In the case of uniform spheres, $R_g = (^3/_5)^{1/2}R_h$, so that $\rho = (^3/_5)^{1/2} = 0.775$; for hollow spheres (vesicles), assuming an infinitely thin wall, $R_g = R_h$, so that $\rho = 1.0$.[40−43] The R_g values of the SA particles coincided with the R_h values, resulting in ρ-values of around 1 (Table 1). SLS data furthermore revealed the molecular weight of the particles, and division by the molecular weight of the monomer resulted in the number of peptides per particle (Table 1). The aggregation number allowed the calculation of the surface area per monomer, assuming an equal distribution of peptides over the inner and outer side of a peptide bilayer.[18] As can be seen in Table 1, the SA7 peptides containing a longer charged hydrophilic domain occupied a larger surface area within the assembly when compared to the SA2 peptides. Furthermore, these assemblies with the larger surface area per peptide also displayed a less negative zeta potential.

pH Dependency of the Self-Assembled Structures. The stability of the SA peptide vesicles was studied as a function of pH by DLS measurements. As can be seen in Figure 5, the peptide assemblies were stable above pH 5.0 as no change in particle size (distribution) was observed. Lowering the pH to 4.0 resulted in the formation of aggregates, as indicated by a dramatic increase in particle size and PDI (Figures 5A and 5C). These aggregates were clearly visible to the naked eye. Reversing the pH to neutral values elicited the formation of self-assemblies of a size and PDI similar to values before acidification (Figures 5B and 5D). Interestingly, hysteresis was observed when reversing the pH values. Whereas destabilization took place around pH 4, reassembly only occurred at pH values ≥7 (Figures 5B and 5D). The vanishing aggregates and appearing assemblies in the reassembly process can also be seen in the DLS size distribution graphs (Figure 5E). At pH 5, large particles were present (1 μm peak) that diminished at pH 6 and were completely gone at pH 7. The size distribution graph after acidification is similar to the initial particle size distribution (Figure 5E).

Calcein Encapsulation. The vesicular nature of the peptide assemblies would allow entrapment of hydrophilic molecules in the interior of the assemblies. To test this, the SA2 assemblies were prepared in the presence of the fluorescent marker calcein. Sephadex G50 size exclusion spin columns were used for rapid separation of the vesicle fraction from non-encapsulated calcein with only minor dilution of the vesicle dispersion, which could potentially destabilize the vesicles.[31] A clear calcein coelution with the assemblies was observed for both SA2 and SA7 peptides, and the degree of calcein entrapment linearly increased with SA peptide concentration (Figure 6). To demonstrate that coelution of calcein with the peptide vesicles is not caused by attachment of calcein to or partitioning into the peptide vesicles, calcein was added to the peptides after assembly. Subsequent spin column separation showed minimal calcein fluorescence in the void volume, comparable to the elution profile of free calcein (Figure S2 of the Supporting Information). As a positive control for calcein encapsulation, negatively charged unilamellar EPG liposomes with comparable size and light scattering intensities as the SA peptide vesicles were used (Figure S2 of the Supporting Information). At a similar light scattering intensity, the degree of calcein encapsulation is 2.5 times lower when compared to negatively charged EPG liposomes.

Discussion

In this study, amphiphilic oligopeptides were recombinantly produced in bacteria and assessed for their self-assembling behavior. Often, solid-phase synthesis is used as a straightforward method for the production of small peptides.[44] However, recombinant production represents a cost-effective alternative to solid-phase synthesis, as it does not require expensive chemicals and can be easily scaled up to gram quantities.[27] Furthermore, the method used for purification of the SA peptides is, in principle, independent of the size, polarity, and charge of the peptide and thus does not require setting up different purification schemes for each peptide when different peptides have to be produced. Recombinant production may also provide means for the extension of peptide lengths toward longer (heteropolymeric) polypeptides.

The use of the intrinsic tryptophan fluorescence of the peptides for CAC determination avoids the need for an external fluorophore, which might interfere with the self-assembling behavior.[45] An increasing CAC with increasing hydrophilic block length was observed, and this trend was confirmed by the CAC value of a peptide containing five glutamic acids. Such an effect has also been observed for other small amphiphilic peptides.[46]

The polydispersity index of the peptide assemblies derived from dynamic light scattering indicated the formation of an ordered structure. This was confirmed by TEM investigations, which revealed highly organized, spherical structures. The particles are formed spontaneously by resuspension of the acid-precipitated peptides, and no sizing by means of extrusion or sonication is required to obtain such a relatively monodisperse size distribution. Further studies by SLS confirmed the vesicular nature of the spherical assemblies. The calculated ρ-values indicated the specific density distribution at the particle edge that is characteristic of a vesicle. Assuming a peptide bilayer, as was proposed by Vauthey et al. for similar amphiphilic peptides,[10] the surface area occupied by the peptides (4.0 nm^2 for SA2 and 8.9 nm^2 for SA7) are in good agreement with values found for other vesicles.[26,47] An increased length of the hydrophilic block indeed resulted in a larger surface area per

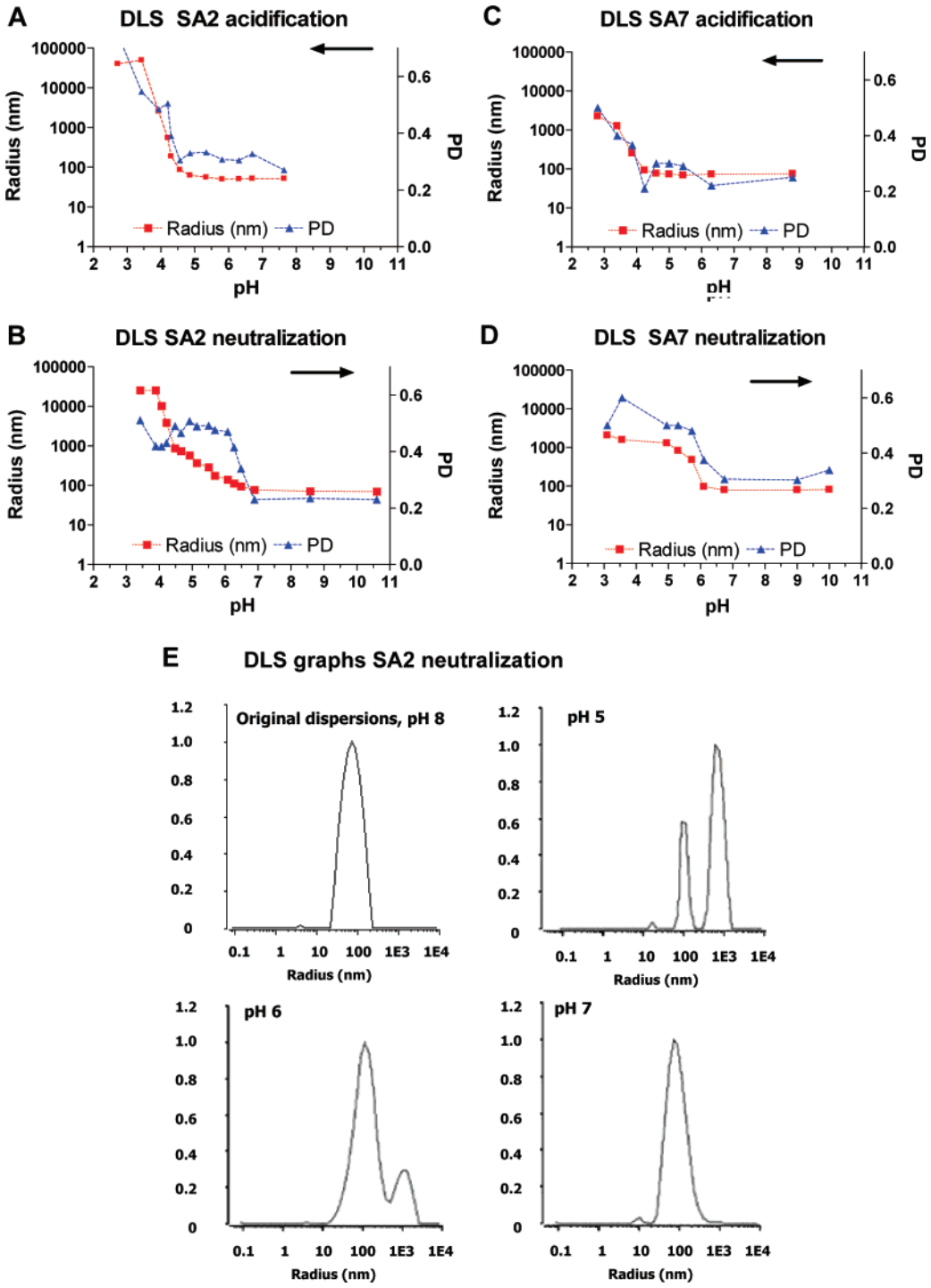

Figure 5. Effect of pH on the size of the SA peptide assemblies, as monitored by DLS measurements. Aggregation of the SA2 and SA7 peptides occurs below pH 4.0. The destabilization process is reversed by neutralization of the pH values, displaying hysteresis and restoring size and PDI to initial values. (E) The process is further visualized by DLS size distribution graphs of SA2 peptides.

monomer, as has been suggested before.[22,24] Surprisingly, the increased hydrophilic mass fraction had no influence on the size and shape of the vesicles.

Furthermore, the vesicular nature of the assemblies was confirmed by their ability to entrap calcein, a small water-soluble fluorescent molecule, inside these peptide vesicles. The quantity of entrapped calcein was positively correlated with the peptide concentration used and was not due to diffusion of calcein into the spherical assemblies, as the addition of equal concentrations of calcein to the peptide vesicles after rehydration yielded much lower calcein fluorescence levels associated with the peptide vesicles (Figure 6). The SA2 vesicles entrapped a somewhat higher amount of calcein. These peptides display a lower CAC than SA7 peptides (Figure 3), and the SA2 peptides within the assembly might be packed denser, resulting in an increased ability to entrap water-soluble compounds. Such a difference in packaging density of SA peptides is supported by the SLS data, which show a larger surface area per monomer for SA7, and by the maximal SA7 anisotropy value, which indicates an increased movement for the SA7 peptides. The quantity of encapsulated calcein in SA2 vesicles is 2.5 times lower compared to the amount entrapped in negatively charged phospholipid vesicles of similar size and comparable scattering intensity. This difference may be related to the preparation

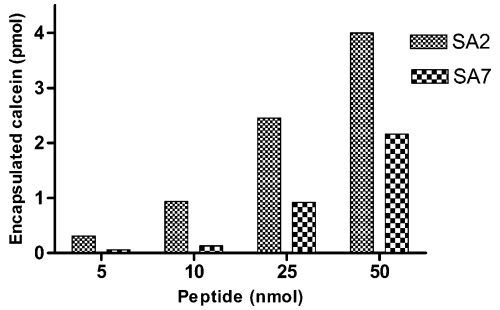

Figure 6. Calcein incorporation in SA2 peptide assemblies. At an increasing amount of peptide, the assemblies were prepared in the presence of a constant calcein concentration.

methods of these two types of vesicles (lipid-film hydration vs precipitate dispersion) or to the amount of vesicles present, since scattering intensity is not only dependent on particle concentration but also on the refractive index of the particles, which may be different for liposomes compared to peptide vesicles.

Interestingly, the self-assembly behaviors of the SA peptides presented here are different from other amphiphilic oligopeptides described, such as G_8D_2 or A_6D, that predominantly form branched nanotubes.[10,11] It might well be that differences in molecular geometry cause differences in the self-assembly of the SA peptides.[23,48] A truncated cone has been proposed as the optimal packaging shape of the monomers in vesicle-forming amphiphiles.[21,23] Such a geometry is influenced by the length of the hydrophobic domain of the amphiphile in relation to the size of the interfacial surface area of the monomer within the assembly,[24,48] which is larger for the SA peptides compared to, for example, G_8D_2 or A_6D, due to the larger glutamic acid side chain. Furthermore, the geometry of the peptide monomers also favors a conical shape as the hydrophobic amino acids increase in size toward the hydrophilic domain.

The spontaneous nature of the self-assembly of peptides into vesicular structures is illustrated by their pH dependency. As studied by DLS measurements, the peptide vesicles aggregate below the pK_a of the side chain carboxyl group of glutamic acid (4.3). It could not be determined whether this aggregation caused disruption of the vesicular assemblies. However, the assembly can be restored by readjusting the pH to neutral or basic values. The observed hysteresis upon pH neutralization might be caused by the shielding of peptides from the environment within the large aggregates, which may hinder deprotonation. Nevertheless, the experiments show that assembly and disassembly of the SA peptide vesicles can be controlled by changing the pH of the surrounding medium, which may be useful for drug delivery applications.

According to the DLVO theory which describes the force between charged surfaces interacting through a liquid medium, the higher the Coulombic repulsion between the particles, the more stable the colloids are.[23,49] The SA2 assemblies display a more negative zeta potential compared to the SA7 assemblies (Table 1), which might favor their long-term stability. Also, SA2 displayed a lower CAC, which is favorable for in vivo applications. An even further decrease of CAC might be established by modification or extension of the hydrophobic block or by enhancement of secondary structure formation.[50]

Conclusion

A versatile method to recombinantly produce amphiphilic peptides in bacteria was developed. It was demonstrated that these SA peptides assemble spontaneously into nanosized vesicles above their critical aggregation concentration at neutral or basic pH. Furthermore, the study elucidates the characteristic of fully reversible assembling process of these peptides when brought into an acidic solution. Interestingly, hydrophilic compounds could be encapsulated within the peptide vesicles and may therefore be useful as drug delivery systems, exhibiting a pH-dependent release profile.

Acknowledgment. We thank Aissa Ramzi, John Kruijtzer, and Ed Moret for their valuable contributions and Kees Steenbeek, Arjen Scholten, and Annemarie Dechense for performing the mass spectrometry analyses. The Electron Microscope Facility of the Department of Biology Utrecht is thanked for the use of their microscopes, and Hans Meeldijk is specially thanked for his comments and assistance.

Supporting Information Available. Additional atomic force microscopy and calcein entrapment experiments. This material is available free of charge via the Internet at http://pubs.acs.org.

References and Notes

(1) Rothemund, P. W. *Nature* **2006**, *440*, 297−302.
(2) Zhang, S.; Marini, D. M.; Hwang, W.; Santoso, S. *Curr. Opin. Chem. Biol.* **2002**, *6*, 865−871.
(3) Aggeli, A.; Bell, M.; Boden, N.; Keen, J. N.; Knowles, P. F.; McLeish, T. C.; Pitkeathly, M.; Radford, S. E. *Nature* **1997**, *386*, 259−262.
(4) Nowak, A. P.; Breedveld, V.; Pakstis, L.; Ozbas, B.; Pine, D. J.; Pochan, D.; Deming, T. J. *Nature* **2002**, *417*, 424−428.
(5) Narmoneva, D. A.; Oni, O.; Sieminski, A. L.; Zhang, S.; Gertler, J. P.; Kamm, R. D.; Lee, R. T. *Biomaterials* **2005**, *26*, 4837−4846.
(6) Hartgerink, J. D.; Beniash, E.; Stupp, S. I. *Proc. Natl. Acad. Sci. U.S.A.* **2002**, *99*, 5133−5138.
(7) Aggeli, A.; Nyrkova, I. A.; Bell, M.; Harding, R.; Carrick, L.; McLeish, T. C.; Semenov, A. N.; Boden, N. *Proc. Natl. Acad. Sci. U.S.A.* **2001**, *98*, 11857−11862.
(8) Rodriguez-Hernandez, J.; Lecommandoux, S. *J. Am. Chem. Soc.* **2005**, *127*, 2026−2027.
(9) Holowka, E. P.; Pochan, D. J.; Deming, T. J. *J. Am. Chem. Soc.* **2005**, *127*, 12423−12428.
(10) Vauthey, S.; Santoso, S.; Gong, H.; Watson, N.; Zhang, S. *Proc. Natl. Acad. Sci. U.S.A.* **2002**, *99*, 5355−5360.
(11) Santoso, S.; Hwang, W.; Hartman, H.; Zhang, S. *Nano Lett.* **2002**, *2*, 687−691.
(12) Hartgerink, J. D.; Beniash, E.; Stupp, S. I. *Science* **2001**, *294*, 1684−1688.
(13) Ellis-Behnke, R. G.; Liang, Y. X.; You, S. W.; Tay, D. K.; Zhang, S.; So, K. F.; Schneider, G. E. *Proc. Natl. Acad. Sci. U.S.A.* **2006**, *103*, 5054−5059.
(14) Zhang, S.; Holmes, T. C.; DiPersio, C. M.; Hynes, R. O.; Su, X.; Rich, A. *Biomaterials* **1995**, *16*, 1385−1393.
(15) Nagai, Y.; Unsworth, L. D.; Koutsopoulos, S.; Zhang, S. *J. Controlled Release* **2006**, *115*, 18−25.
(16) Garreta, E.; Genove, E.; Borros, S.; Semino, C. E. *Tissue Eng.* **2006**, *12*, 2215−2227.
(17) von Maltzahn, G.; Vauthey, S.; Santoso, S.; Zhang, S. U. *Langmuir* **2003**, *19*, 4332−4337.
(18) Tsai, C. J.; Zheng, J.; Nussinov, R. *PLoS Comput. Biol.* **2006**, *2*, e42.
(19) Crommelin, D. J.; Storm, G. *J. Liposome Res.* **2003**, *13*, 33−36.
(20) Holowka, E. P.; Sun, V. Z.; Kamei, D. T.; Deming, T. J. *Nat. Mater.* **2007**, *6*, 52−57.
(21) Israelachvili, J.; Mitchell, D.; Ninham, B. *J. Chem. Soc., Faraday Trans. 2* **1976**, *72*, 1525−1568.
(22) Rovira-Bru, M.; Thompson, D. H.; Szleifer, I. *Biophys. J.* **2002**, *83*, 2419−2439.
(23) Israelachvili, J. *Intermolecular and Surface Forces*, 2nd ed.; Academic Press: London, 1991; pp 366−394.
(24) Discher, D. E.; Eisenberg, A. *Science* **2002**, *297*, 967−73.
(25) Riley, T.; Stolnik, S.; Heald, C. R.; Xiong, C. D.; Garnett, M. C.; Illum, L.; Davis, S. S.; Purkiss, S. C.; Barlow, R. J.; Gellert, P. R. *Langmuir* **2001**, *17*, 3168−3174.
(26) Discher, B. M.; Won, Y. Y.; Ege, D. S.; Lee, J. C.; Bates, F. S.; Discher, D. E.; Hammer, D. A. *Science* **1999**, *284*, 1143−1146.
(27) Reed, D. C.; Barnard, G. C.; Anderson, E. B.; Klein, L. T.; Gerngross, T. U. *Protein Expression Purif.* **2006**, *46*, 179−188.

(28) Fass, R.; Vandewalle, M.; Shiloach, A.; Joslyn, A.; Kaufman, J.; Shiloach, J. *Appl. Microbiol. Biotechnol.* **1991**, *36*, 65−69.
(29) Lemmel, C.; Weik, S.; Eberle, U.; Dengjel, J.; Kratt, T.; Becker, H. D.; Rammensee, H. G.; Stevanovic, S. *Nat. Biotechnol.* **2004**, *22*, 450−454.
(30) Pencer, J.; Hallett, F. R. *Langmuir* **2003**, *19*, 7488−7497.
(31) Fry, D. W.; White, J. C.; Goldman, I. D. *Anal. Biochem.* **1978**, *90*, 809−815.
(32) Olson, F.; Hunt, C. A.; Szoka, F. C.; Vail, W. J.; Papahadjopoulos, D. *Biochim. Biophys. Acta* **1979**, *557*, 9−23.
(33) Killian, J. A.; von Heijne, G. *Trends Biochem. Sci.* **2000**, *25*, 429−434.
(34) Carstens, M. G.; Bevernage, J. J. L.; van Nostrum, C. F.; van Steenbergen, M. J.; Flesch, F. M.; Verrijk, R.; de Leede, L. G. J.; Crommelin, D. J. A.; Hennink, W. E. *Macromolecules* **2007**, *40*, 116−122.
(35) Yoo, Y.; Rote, K.; Rechsteiner, M. *J. Biol. Chem.* **1989**, *264*, 17078−17083.
(36) Malakhov, M. P.; Mattern, M. R.; Malakhova, O. A.; Drinker, M.; Weeks, S. D.; Butt, T. R. *J. Struct. Funct. Genomics* **2004**, *5*, 75−86.
(37) Butt, T. R.; Edavettal, S. C.; Hall, J. P.; Mattern, M. R. *Protein Expression Purif.* **2005**, *43*, 1−9.
(38) Lakowicz, J. *Principles of Fluorescence Spectroscopy*, 3rd ed.; Springer: New York, 2006.
(39) Kastantin, M.; Ananthanarayanan, B.; Lin, B.; Ressl, J.; Black, M.; Tirrell, M. *Macromol. Biosci.* **2007**, *7*, 189−194.
(40) Benoit, H.; Froehlich, D. In *Light Scattering from Polymer Solutions*; Huglin, M. B., Ed.; Academic Press: London, 1972; pp 520−535.
(41) Burger, C.; Hao, J.; Ying, Q.; Isobe, H.; Sawamura, M.; Nakamura, E.; Chu, B. *J. Colloid Interface Sci.* **2004**, *275*, 632−641.
(42) Nie, T.; Zhao, Y.; Xie, Z. W.; Wu, C. *Macromolecules* **2003**, *36*, 8825−8829.
(43) Carstens, M. G.; van Nostrum, C. F.; Ramzi, A.; Meeldijk, J. D.; Verrijk, R.; de Leede, L. L.; Crommelin, D. J.; Hennink, W. E. *Langmuir* **2005**, *21*, 11446−11454.
(44) Merrifield, R. B. *J. Am. Chem. Soc.* **1963**, *85*, 2149−2154.
(45) Jones, G.; Vullev, V. I. *Org. Lett.* **2001**, *3*, 2457−2460.
(46) Yang, S. J.; Zhang, S. G. *Supramol. Chem.* **2006**, *18*, 389−396.
(47) Gao, W. P.; Bai, Y.; Chen, E. Q.; Li, Z. C.; Han, B. Y.; Yang, W. T.; Zhou, Q. F. *Macromolecules* **2006**, *39*, 4894−4898.
(48) Antonietti, M.; Forster, S. *Adv. Mater.* **2003**, *15*, 1323−1333.
(49) Kayes, J. B. *J. Pharm. Pharmacol.* **1977**, *29*, 199−204.
(50) Vandermeulen, G. W.; Klok, H. A. *Macromol. Biosci.* **2004**, *4*, 383−398.

BM0704267